Fırat Üniversitesi Deneysel ve Hesaplamalı Mühendislik Dergisi

FUJECE

$LiNiO_2$'nin Performans Geliştirmesi İçin Mn ve Ti Eş Katkısı

Erdinç ÖZ[1,2*], Jeff DAHN[3]

[1] Fizik Bölümü, Fen Fakültesi, Atatürk Üniversitesi, Erzurum, Türkiye.
[2]Nanobilim ve Nanomühendislik Anabilimdalı, Fen Bilimleri Enstitüsü, Atatürk Üniversitesi, Erzurum, Türkiye.
[3]Fizik ve Atmosferik Bilimler Bölmü, Dalhousie Üniversitesi, Halifax, Kanada.
[1,2]erdinc.oz@atauni.edu.tr, [3]jeff.dahn@dal.ca

Geliş Tarihi: 27.03.2024
Kabul Tarihi: 29.05.2024

Düzeltme Tarihi: 24.05.2024

doi: 10.62520/fujece.1459826
Araştırma Makalesi

Alıntı: E. Öz ve J. Dahn, "Linio2'nin performans geliştirmesi için mn ve ti eş katkısı", Fırat Üni. Deny. ve Hes. Müh. Derg., vol. 3, no 3, pp. 280-291, Ekim 2024.

Öz

$LiNiO_2$ (LNO) yüksek kapasiteye sahiptir ancak lityum-iyon pillerde pratik kullanımını sınırlayan yapısal istikrarsızlık ve kapasite azalmasından muzdariptir. Bu çalışma, bu sorunların üstesinden gelmek için bir strateji olarak LNO yapısındaki Ni bölgelerine Mn ve Ti birlikte katkılayarak $LiNi_{0.95}Mn_{0.025}Ti_{0.025}O_2$ (MnTi25) elde etmeyi ve fiziksel ve elektrokimyasal özelliklerini araştırmayı önermektedir. MnTi25, LNO'ya kıyasla gelişmiş yapısal kararlılık ve önemli ölçüde azaltılmış katyon karışımını ortaya çıkararak kayda değer elektrokimyasal sonuçlar vermiştir. MnTi25'in yarı hücre performansı etkileyicidir ve yerleşik %4 Mn ikameli ZoomWeMn4 standardına benzer bir kapasite sergileyerek etkili Li-iyon çıkarma ve ekleme işlemini göstermektedir. Ayrıca, grafit anoda karşı yapılan tam hücre testi, MnTi25'in ticari bir LNO bazlı malzeme ile neredeyse aynı kapasiteyi sunduğunu göstermektedir. Bu kayda değer başarı, yüksek kapasite potansiyelini korurken LNO'nun sınırlamalarını ele almada ortak katkının etkinliğini vurgulamaktadır. Bu çalışma, MnTi25'in, malzemenin yapısını Mn ve Ti birlikte katkılama yoluyla uyarlayarak yüksek performanslı lityum-iyon piller için umut verici bir katot malzemesi olabileceğini göstermektedir.

Anahtar kelimeler: Lityum-iyon bataryalar, Mn ve Ti çift katkılama, Geliştirilmiş yapısal kararlılık

*Yazışılan yazar

İntihal Kontrol: Evet– Turnitin
Şikayet: fujece@firat.edu.tr

Firat Univ Jour. of Exp. and Comp. Eng., 3(3), 280-291, 2024

Firat University Journal of Experimental and Computational Engineering

FUJECE

Mn and Ti Co-doping of $LiNiO_2$ to Improve Performance

Erdinc OZ[1,2*], Jeff DAHN[3]

[1]Physics Department, Faculty of Science, Atatürk University, Erzurum, Türkiye.
[2]Nanoscience and Nanoengineering Department, Institute of Science, Atatürk University, Erzurum, Türkiye.
[3]Department of Physics & Atmospheric Science, Department of Chemistry, Dalhousie University, Halifax, Canada.
[1,2]erdinc.oz@atauni.edu.tr, [3]jeff.dahn@dal.ca

Received: 27.03.2024
Accepted: 29.05.2024

Revision: 24.05.2024

doi: 10.62520/fujece.1459826
Research Article

Citation: E. Oz ve J. Dahn, "Mn and Ti Co-doping of $LiNiO_2$ to Improve Performance", Firat Univ. Jour.of Exper. and Comp. Eng., vol. 3, no 3, pp. 280-291, October 2024.

Abstract

$LiNiO_2$ (LNO) has high capacity but suffers from structural instability and capacity fade, which limits its practical use in lithium-ion batteries. This study proposes co-doping LNO with Mn and Ti (MnTi25) as a strategy to overcome these issues. MnTi25 was thoroughly characterized, revealing improved structural stability and significantly reduced cation mixing compared to pristine LNO. The half-cell performance of MnTi25 is noteworthy, exhibiting a capacity similar to the established 4% Mn-substituted ZoomWeMn4 standard, demonstrating efficient Li-ion extraction and insertion. Additionally, full-cell testing against a graphite anode shows that MnTi25 delivers a capacity almost identical to a commercial LNO-based material. This promising achievement highlights the effectiveness of co-doping in addressing LNO's limitations while preserving its high-capacity potential. This study demonstrates that MnTi25 can be a promising cathode material for high-performance lithium-ion batteries by tailoring the material's structure through co-doping.

Keywords: Lithium-ion batteries, Mn and Ti dual doping, Improved structural stability

*Corresponging author

1. Introduction

Lithium-ion batteries (LIBs) reign supreme in portable electronics due to their high energy density and impressive cycle life. However, realizing their full potential for electric vehicles and grid storage demands further advancements in these aspects. In this quest, Ni-rich layered $LiNiO_2$ (LNO) cathodes hold immense promise, boasting a theoretical capacity surpassing 275 mAh g^{-1} [1], significantly exceeding conventional $LiCoO_2$. Despite their alluring potential, practical application remains hindered by inherent drawbacks such as structural instability, voltage fade, and thermal instability, primarily stemming from Ni cation migration and oxygen loss. For example, according to the study by Yoon et al. [2], H2 - H3 phase transformations occurred in $LiNiO_2$ particles at 4.2 and 4.3V cut-off voltage levels, causing structural instabilities, and as a result, microcracks were observed on the particle surfaces. These cracks not only adversely affect ionic and electronic transport, causing performance losses, but also cause the electrolyte to diffuse into the particle interior, rendering the particle surface useless for redox reactions. Another situation is that when $LiNiO_2$ is in the state of charge (delithiation), Ni^{4+} is highly reactive and reacts with the electrolyte after Li ions leave the crystal structure. In this case, the $LiNiO_2$ phase usually decomposes into more stable $Li_{\&}Ni_{1-\&}O_2$ phases, O_2 and NiO [3], [4]. Different strategies such as substitution/doping of Fe [5], Al [6], and Co [7] into the crystal structure or surface coating with MgO [8], Silica [9], and $AlPO_4$ [10] have been tried to prevent these negative properties of NRO. However, surface coating may also increase the weight and volume of the battery, reducing its energy and power density. Surface coating may also cause interface resistance, coating cracking, or coating peeling, which may affect the cycling performance and the rate capability of the battery [11, 12].

Co-doping represents a noteworthy approach whereby two distinct atomic species within the material matrix concurrently manifest advantageous physical and electrochemical characteristics, while also offsetting each other's inherent limitations. One of the studies on co-doping LNO is on $LiNi_{0.990}Al_{0.005}Ti_{0.005}O_2$ sample synthesized by wet milling solid-state reaction method by Song et al [13]. Performance tests showed an initial capacity of 196.3 mAh/g at a current density of 0.1C and a voltage range of 2.2 - 4.4V. On the other hand, it decreased to 113.8 mAh/g capacity after 20 cycles and showed 57.9% capacity retention. Zhou and Zheng et al. conducted another investigation on the co-doping of Mg and Al into LNO [14]. They demonstrated that the co-doping of Mg and Al inhibits the coalescence of secondary particles and facilitates Li diffusion by expanding the interlayer spacing. Based on their findings, they identified $LiNi_{0.95}Al_{0.04}Mg_{0.01}O_2$ as the optimal composition, which exhibits an initial capacity of 200.8 mAh/g and a capacity retention of 83.7% after 200 cycles at 0.5C.

Addressing these limitations has spurred extensive research into doping LNO with transition metals. Among the contenders, Mn and Ti stand out for their unique and complementary benefits: Sharing a similar ionic radius and oxidation state with Ni^{2+}, Mn^{4+} holds the potential to mitigate cation migration and stabilize the layered structure. Moreover, Mn redox contributes to the overall capacity, enhancing the theoretical energy density. For instance, Arai et al. reported 10% Mn substitution as the upper limit and obtained an initial capacity of 200 mAh/g in performance tests [15]. However, their study also highlighted the need for further optimization to address the voltage polarization observed and capacity fade after 10 cycles. Another important advantage of Mn over other dopants is its abundance and low cost [16]. Additionally, previous studies have reported that the positive effect of Mn doping on the thermal stability of LiNiO2 cathode material is similar to that of Ti and far superior to that of Co doping [17]. With its exceptional oxygen affinity, Ti^{4+} can act as an "electronic pillar," stabilizing the Ni oxidation state and reducing voltage fade. In contrast, Ti^{4+} ions exhibit a greater preference for occupying transition metal (Mn^{4+}, Ni^{3+}, etc.) sites compared to Li^+ sites. This preference arises from the differing energetic costs associated with substituting Li^+ or transition metals with Ti^{4+} at these distinct lattice positions. The substitution of Ti^{4+} into transition metal sites leads to an expansion of the interplanar spacing and unit cell volume, which can facilitate the lithium insertion/extraction process [18]. Kim and Amine prevented the migration of Ni^{2+} ions to the Li sites by substituting Ti^{4+} for Ni sites in $LiNiO_2$. This reduced the capacity loss by decreasing the cation mixing ratio [19]. Their results showed that $LiNi_{1-x}Ti_xO_2$ ($0.025 < x < 0.2$) materials had an initial capacity of 240 mAh/g and maintained high-capacity retention after 100 cycles. It is important to note that if the Ti substitution rate exceeds x=0.25, the Ni^{2+} ions formed for charge balancing will begin to occupy the Li sites, resulting in a

loss of capacity. Additionally, highly substituted Ti ions may settle between the layers of the crystal structure instead of occupying Ni sites, which could negatively impact both ionic and electronic diffusion.

While previous studies have explored the individual merits of Mn and Ti doping on LNO, their independent approaches may not fully address the multifaceted challenges faced by these cathodes. Recognizing this gap, this study delves into the synergistic effects of co-doping LNO with 0.25 mol Mn and 0.25 mol Ti on the cathode material's physical and electrochemical performances. By systematically characterizing the doped LNO material and evaluating its electrochemical performance, we aim to contribute to the development of high-performance Ni-rich cathodes, advancing the potential of LIBs for next-generation energy storage applications.

2. Material and Method

2.1. Material Synthesis

In the context of our experimental investigation, we synthesized the $Ni_{0.974}Mn_{0.026}(OH)_2$ precursor using the co-precipitation method within a continuously stirred tank reactor (CSTR) (Brunswick Scientific/Eppendorf BioFlo 310). The principal advantages of the coprecipitation method are the simultaneous mixing of transition metals at the atomic level, the achievement of the requisite phase and crystallization at relatively mild sintering temperatures, and the retention of time [20]. Aqueous solutions of $Ni(SO_4{\cdot}6H_2O)$ (98%, Alfa Aesar) and $Mn(SO_4)$ (98%, Alfa Aesar) were meticulously prepared, maintaining the specified Ni:Mn molar ratios. The Nickel and Manganese reagents were combined into a single solution (400 mL, 2 M). Subsequently, these solutions were added dropwise in a simultaneous manner, utilizing peristaltic pumps, to a stirred reaction vessel containing NH_3 solution (1 L, 1 M). To maintain a precise pH concentration (pH 11.0 and 0.5 M NH_3), we introduced a NaOH solution (98%, Alfa Aesar) (10 M) and an NH_3 solution (5 M). For 20 hours, the solutions were gradually incorporated into the reaction vessel, which was maintained at 60 °C, stirred at 900 rpm, and placed under an N_2 atmosphere. Following the reaction, the vessel was cooled to room temperature, and the resulting precipitate was meticulously filtered and rinsed four times with deionized water. Finally, the precipitate was dried overnight at 100 °C in ambient air (Figure 1a).

The process of inserting Li into the precursor crystal structure is called "lithiation". In this step, the precursor and a lithium source are physically mixed and heat-treated at high temperature. Carbonate or hydroxide compounds can be used as lithium sources. The lithiation step was carried out for Li_2CO_3:$Ni_{0.974}Mn_{0.026}(OH)_2$: TiO_2 using the 1.02:0.95:0.025 ratios. In the first lithiation step, the samples were ground by hand, heat treated at 480 ^oC for 3 hours, and cooled to room temperature. The objective of this step is to remove carbonate from Li2CO3 and water from the $Ni_{0.974}Mn_{0.026}(OH)_2$. Then the samples were ground again by hand for 15 minutes and then heated up at 825 ^0C for 20 hours in O_2 atmosphere. The purpose of the second lithiation step is to allow Li^+, Ti^{+4} and O_2 released from the Li source to diffuse into the $Ni_{0.974}Mn_{0.026}(OH)_2$ (Figure 1b).

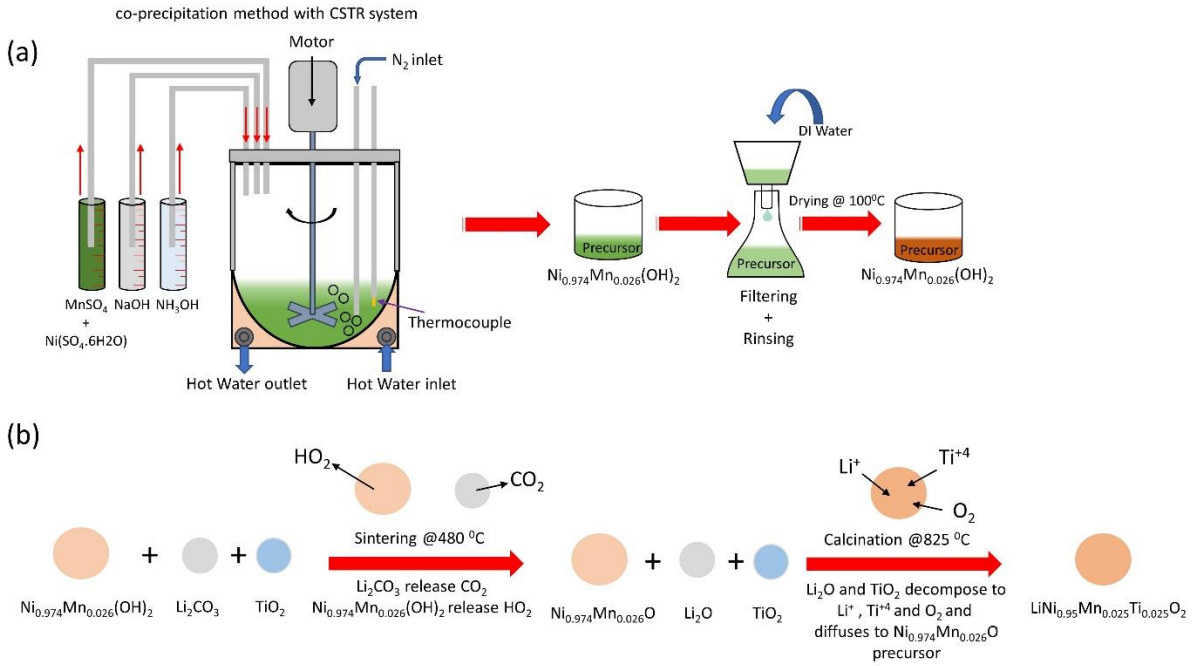

Figure 1. (a) Synthesis process of precursor by co-precipitation using CSTR. (b) Schematic representation of the lithiation step of the precursor

To compare the MnTi25 sample with a standard sample, $Ni_{0.96}Mn_{0.04}(OH)_2$ precursor was obtained from ZoomWe (Hunan ZoomWe Zhengyuan Advanced Material Trade Company, Ltd., Changsha 410000, China). To obtain $LiNi_{0.96}Mn_{0.04}O_2$ (ZoomWeMn4), the same lithiation steps as MnTi25 were applied.

2.2. Physical Characterization

X-ray diffraction (XRD) patterns were acquired using a Siemens D5 diffractometer equipped with a copper (Cu) target X-ray tube and a diffracted beam monochromator. The samples were meticulously analyzed within a scattering angle (2θ) range from 15° to 80°, with data collection intervals of 0.02° over 3 seconds. Scanning electron microscopy (SEM) imaging was conducted using a Hitachi S4700 Scanning Electron Microscope equipped with a backscattered electron detector. Before imaging, the samples were meticulously prepared by affixing the powders onto adhesive carbon tape. The resulting images were captured under an accelerating voltage of 3 kV and a current of 20 µA. Particle size analyses of the samples were made with a Partica laser scattering particle size distribution analyzer (Horiba). An ICP-MS (Thermo Fisher Scientific, MA, USA) paired with an ESI SC-4DXS autosampler (Elemental Scientific, NE, USA) was used for sample elemental distribution analysis. Standard samples of the elements to be measured were prepared as 4ppm, 2ppm, and 1ppm standards.

2.3. Electrochemical Characterization

A mixture was made by Super-S carbon black (Timcal) as the active material, polyvinylidene fluoride (PVDF, Arkema, Kynar 301F) as the binder, and N-methyl-2-pyrrolidone (NMP, Sigma-Aldrich, 99.5%) as the solvent in a weight ratio of 92:4:4. The resulting slurry was coated onto aluminum foil using a 150 µm high-adjustable doctor blade and dried in a vacuum oven at 110 °C. The dried electrodes were then calendared under pressure and punched into circular discs (1.25 cm diameter) with an electrode material loading of 10–12 $mg.cm^{-2}$. The discs were subsequently dried overnight in a vacuum at 110 °C.

For the half-cell performances, positive electrodes were used as cathode, Li metal as anode material, and Celgard 2032 membrane as a separator with the electrolyte of 1.2 M $LiPF_6$ (BASF, 99.9%) in a mixture of

fluoroethylene carbonate (FEC) and dimethyl carbonate (DMC) was used as the electrolyte (FEC: DMC 1:4 v/v). A 2032 type coin cell battery was used for the tests and all assemblies were performed in an Ar-filled glove-box.

For full cells, the negative/positive electrode capacitance ratio should be 1.0-1.5. Outside this range, rapid capacity losses are observed in full cells. During the production of the positive electrode, the mixing ratios stated above for the half-cell were used. For slurry to be used more efficiently during coating, the total solid mixture/NMP ratio varies between 1.0 and 1.5. Graphite (Novonix) with a capacity of 3 mAh/cm^2 coated on copper foil was used as the negative electrode in full cells. The discs used as negative electrodes were punched to be 12.75 mm in diameter. Since the punched discs for the positive electrode have a constant radius (11.25 mm) and to provide the N/P ratio in full cells, different thicknesses were tried during the coating of the slurry on aluminum foil. 1.2 M $LiPF_6$ in EC: DMC 3:7 w/w were used as electrolyte. In addition, 2%FEC and 1%LFO (lithium difluorophosphate) were added to the electrolyte solution. About 10 microliters of electrolyte are used in each battery. BMF (Polypropylene Blown Micro Fiber available from 3M Company) separator was used as a membrane. Since this membrane has a thicker structure compared to Celgard, a one-piece BMF membrane disc was used in each battery.

3. Results and Discussions

Figure **2** shows the XRD patterns of the powder samples obtained after the final heat treatment. Both samples were found to be isostructural with $LiNiO_2$, which has a rhombohedral layered structure (R-3m)[21]. The XRD peaks of the commercial standard ZoomWeMn4 sample and the MnTi25 samples are identical, as shown in Figure 1a. The MnTi25 sample is very similar to the standard in the separation of the (018) and (110) peaks, which is indicative of good crystallization (Figure 2b). However, no impurity peak was observed in the impurity region of both samples (Figure 2c). The crystal structure and refinement parameters are shown in Table 1. The results of the calculations indicate that the *a* lattice parameter of the MnTi25 sample increased by 0.31% and the *c* parameter increased by 0.27% in comparison to the standard ZoomWeMn4 sample.

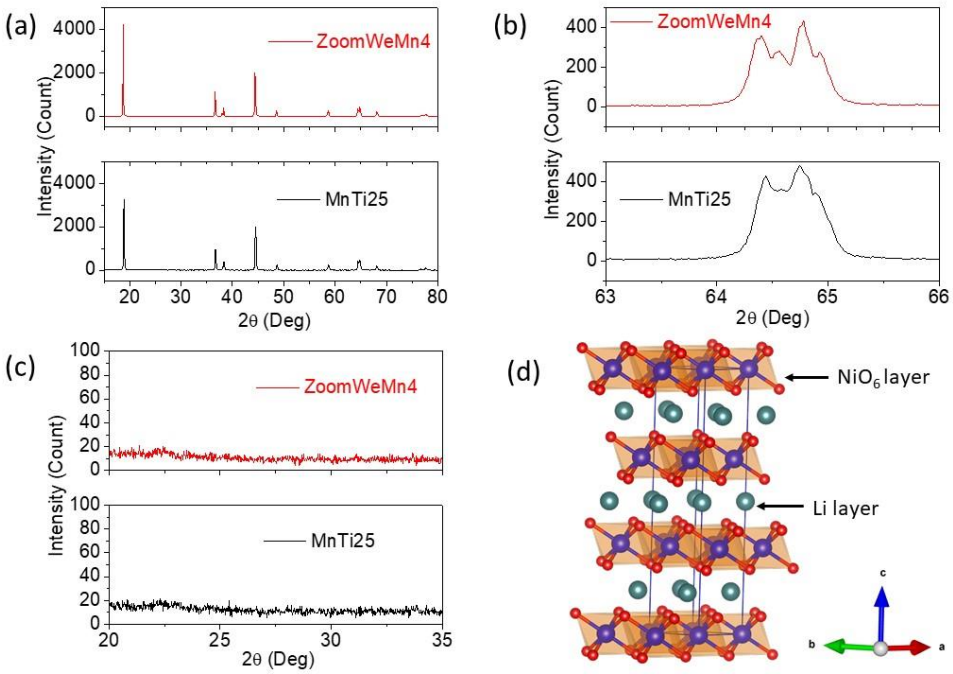

Figure 2. (a) XRD diffraction patterns of MnTi25 and ZoomWe Mn4 samples. (b) Peak splitting of (018) and (110) reflections, indicating the degree of crystallization. (c) Impurity region from 20 to 30°. (d) Layered structure of $LiNiO_2$ crystal, plotted using refinement results

LNO has a layered structure consisting of Li and NiO_6 layers (Figure 2d). To maintain charge neutrality, Ni^{3+} ions are inherently present within the crystal lattice. However, during the synthesis process, Ni^{2+} ions are generated and exhibit a propensity to migrate toward the Li layers—a phenomenon commonly referred to as 'cation mixing' (Ni_{Li}) [22]. Notably, due to the distinct ionic radii of Ni^{2+}, which is larger than that of Ni^{3+} and smaller than that of Li^+, the incorporation of Ni^{2+} within the crystal structure results in contrasting effects. Specifically, the Li plates shrink, while the Ni plates expand [23]. This negatively affects the Li diffusion into the crystal structure during charge/discharge cycles. Previous studies have reported that Mn substitution into Ni sites in $LiNiO_2$ predominantly results in the Mn^{4+} oxidation state [24]. This substitution leads to a discernible increase in *c* (three times the interslab distance) parameters, attributed to the smaller ionic radius of Mn^{4+} compared to Ni^{3+}. On the other hand, the Ti tends to exist in $LiNiO_2$ as Ti^{4+}, which is more stable than Ti^{3+}, and the ionic radius of Ti^{4+} is larger than that of Ni^{3+} [23], Ti^{4+} substituting Ni sites causes an increase in the crystal structure parameters. However, an increase in the incorporation of both Ti^{4+} and Mn^{4+} leads to enhanced cation mixing within the crystal lattice, due to the induced transformation of Ni^{3+} to Ni^{2+} to maintain charge balance. Consequently, an increase in the Ni_{Li} cation mixture was observed, but *c/a*, an indicator of trigonal distortion, decreased.

Table 1. The Lattice and the Refinement parameters of the samples

	Lattice parameters				**Refinement parameters**	
Sample	*a=b* (Å)	*c* (Å)	*c/a*	χ^2	R_{wp}	Ni_{Li} (%)
ZoomWe Mn4	2.872	14.183	4.938	0.624	13.02	0.7
MnTi25	2.881	14.221	4.936	0.685	12.51	4.9

SEM images of the samples at different magnifications are presented in Figure 3. The $Ni_{0.974}Mn_{0.026}(OH)_2$ precursor, obtained through CSTR, exhibits a spherical structure (Figure 3a). The precursors are formed by the aggregation of smaller primary particles while forming the spherical structure, as seen in the figure. The overall structure of the samples is homogeneously distributed and has a similar spherical structure (Figure 3b). After the lithiation step, the MnTi25 sample maintained its spherical structure but transformed into a more rectangular shape due to the addition of Li to the primary particles (Figure 3c). The sample's particle distribution consists of spherical structures with a uniform distribution (Figure 3d).

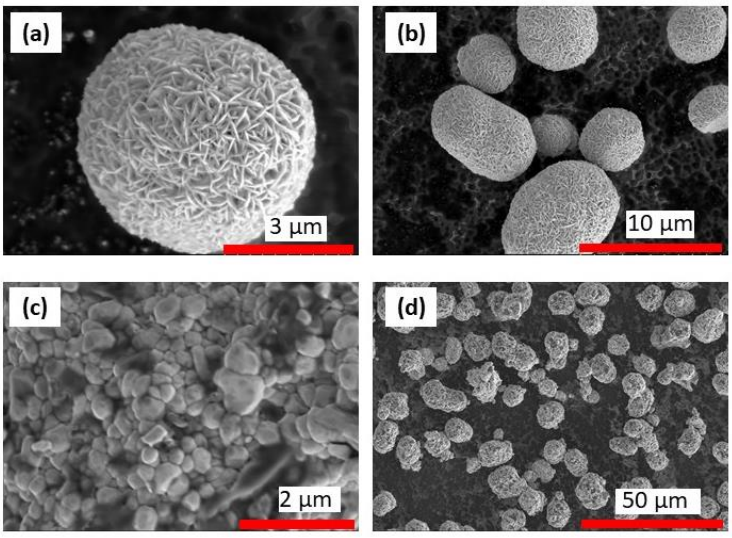

Figure 3. SEM image in different magnifications of precursors (a)-(b), and MnTi25 samples (c)-(d)

The ICP-MS measurements were used to analyze the atomic ratios of all elements in the samples. The atomic ratios of Li:Ni:Mn:Ti in standard ZoomWeMn4 and MnTi25 are 1.057:1.938:0.0417:0 and 1.073:0.945:0.0279:0.0267, respectively, which are very close to the desired stoichiometries. Figure 4 shows the average particle size distribution of the samples. The average particle size of the ZoomWeM4 material used as a commercial standard is observed to be 15 μm with a single peak, while the MnTi25 sample has approximately 10 μm (75%) and 92 μm (25%) with double peaks. This can be seen as an indication that some secondary particles agglomerate to form larger secondary particles.

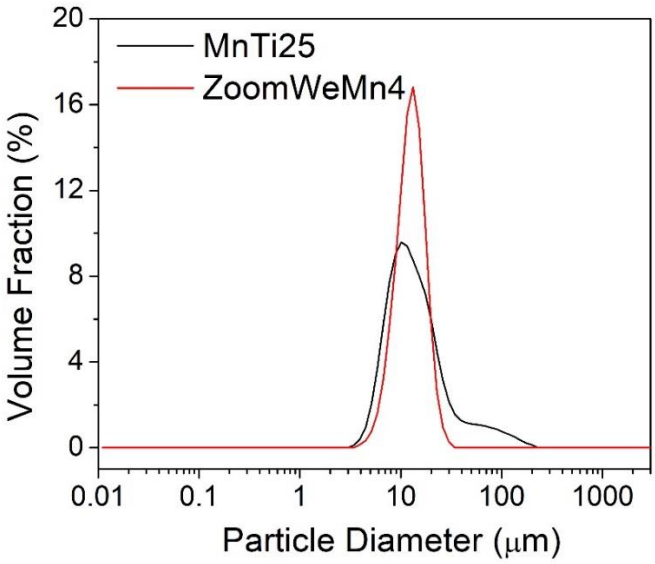

Figure 4. Particle size distribution of the standard ZoomWeMn4 and MnTi25 samples

Figure 5 shows the differential capacity as a function of voltage, half-cell cyclic, and current density performances of standard ZoomWeMn4 and MnTi25. The redox peaks observed in the dQ/dV profiles correspond to multiple phase transitions in the material (Figure 5a-b). These transitions are associated with abrupt changes in the lattice parameters, such as contraction and expansion, and the ordering of lithium ions and vacancies within the crystal structure [25]. In the cathode material composed of lithium nickel oxide (LNO), as lithium ions depart from the crystal lattice, the structural arrangement undergoes a sequence of transitions: hexagonal (H1) to monoclinic (M), followed by another transition to hexagonal (H2), and finally to hexagonal (H3) [25], [26] (Figure 5a-b). Sharp redox peaks in the dQ/dV curves typically signify abrupt and potentially harmful structural alterations. Therefore, a broad redox peak with diminished intensity, which suggests an extended phase transition, is more desirable for maintaining structural stability [27], [28]. When considering this, it is clear that the broader redox peaks of MnTi25 indicate suppression of abrupt phase transitions. Furthermore, the intensity of the redox peak that represents the H2 ⇄ H3 phase transition at ~4.1V, which is considered to be responsible for the loss of LNO capacity [29], [30], is reduced in MnTi25.

The long cycle and Coulombic efficiency performances of the samples are shown in Figure 5c. The MnTi25 cathode performance starts with a specific capacity of 196.6 mAh/g while the standard cathode starts with 194.4 mAh/g. After 100 cycles, the MnTi25 and standard cathode have a specific capacity of 166.7 mAh/g and 164.5 mAh/g, respectively. This result shows that MnTi25 and standard cathode materials have 84.8% and 84.6% capacity retention, respectively. On the other hand, both cathode materials consistently deliver 99% Coulombic efficiency over 100 cycles.

A comparison of the current density performance of the cathode materials at C/20, C/10, C/5, C, and 2C is presented in Figure 5d. The rate capacity graphs of both samples exhibit similar values and a consistent change trend. At a current density of C/20, the MnTi25 and ZoomWeMn4 samples demonstrated capacities of 210.18 mAh/g and 212.86 mAh/g, respectively. However, upon increasing the current density to 2C, a notable decrease in capacity was observed. Specifically, the capacities of the MnTi25 and ZoomWeMn4 samples diminished to 179.63 mAh/g and 183.50 mAh/g, respectively. This phenomenon signifies a capacity retention of 85.5% for MnTi25 and 86.2% for ZoomWeMn4 when the current density was amplified by 40. However, it's worth noting that the MnTi25 sample exhibits a very notable capacity retention. Despite the increase in current density by a factor of 40, MnTi25 manages to retain over 85.5% of its capacity. This is a significant performance characteristic, indicating the stability of MnTi25 under conditions of increased current density.

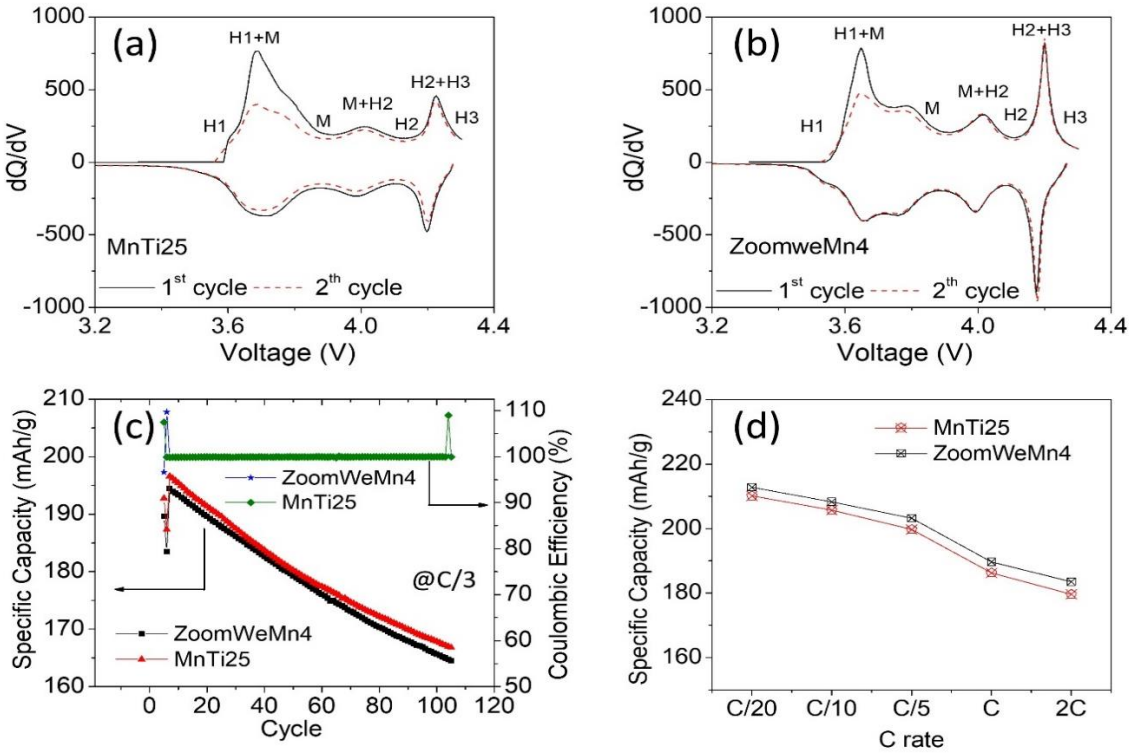

Figure 5. Capacity performance of MnTi25 and ZoomWe Mn4 samples within 3.0 - 4.3V: (a) cycling stability and Coulombic efficiency at C/3 current density for 100 cycles, (b) rate capability at various current densities, and (c) normalized capacity as a function of cycle number

Figure 6 shows the comprehensive depiction of formation cycles at C/20 and full cell performance of the samples against the graphite anode in the voltage range of 3.0-4.2 V at C/3 current density. The first two formation charge/discharge cycles of MnTi25 and ZoomWeMn4 samples at C/20 are shown in Figures 6a and b. During the initial operation of the cells, formation cycles are applied to ensure the controlled formation of the Solid Electrolyte Interphase (SEI). The loss of Li due to irreversible reactions on graphite is referred to as 'irreversible capacity loss' and is considered a loss of cell capacity. The hysteresis observed during the formation cycles at 3.0 V may indicate irreversible capacity loss. An increase in hysteresis is indicative of an increase in capacity loss between cycles. The narrow hysteresis observed in the MnTi25 sample (Figure 6a), similar to the standard sample (Figure 6b), indicates a low level of irreversible capacity loss. The performance graphs (Figure 6c) show that the MnTi25 sample starts with a capacity of 190.8 mAh/g and maintains 178.5 mAh/g over 50 cycles, demonstrating a capacity retention of 93.7%. Similarly, the ZoomWeMn4 sample begins with a capacity of 188.8 mAh/g, holds 176.5 mAh/g after the cycles, and shows a capacity retention of 93.5%.

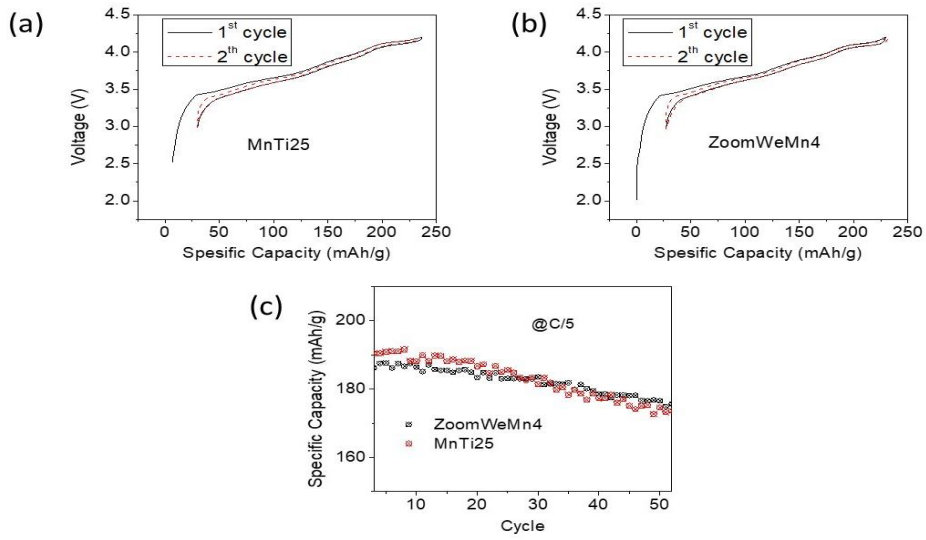

Figure 6. Initial full-cell charge/discharge curves of (a) MnTi25 and (b) ZoomWe Mn4 samples at C/20 current density within 3.0-4.2V. (c) The performance capacity of the samples for 50 cycles at a C/5 current density

The decrease in capacity performance of MnTi25 can be attributed to the increase in cation mixing: Substituting Mn^{4+} and Ti^{4+} reduces Ni^{3+} to Ni^{2+} to maintain charge balance. Li^{+} ions leave the crystal structure and form vacancies during charging, and some Ni^{2+} ions can migrate from transition metal slabs into these vacancies due to their similar radii to Li^{+}, and increase the cation mixing. The migration of Ni^{2+} ions into vacancies prevents Li^{+} ion diffusion into slabs and migration into vacancies during discharge, resulting in capacity loss. Another factor is that Mn^{4+} and Ti^{4+} ions are electrochemically inactive and do not contribute to the redox reactions [24], [31]. However, considering both half-cell and full-cell performances, Mn and Ti co-substitution improved capacity retention. When comparing the two samples, the Mn content of MnTi25 is reduced compared to the standard sample and Ti is substituted instead. The fact that the capacity retention of the MnTi25 sample is noticeably higher in battery performance tests demonstrates that the Ti substitution makes a positive contribution to performance. This is explained by the fact that although Ti is electrochemically inactive, the Ti-O bonds are stronger than the Ni-O and Mn-O bonds and prevent degradation of the crystal structure during charging/discharging [32].

4. Conclusion

In this study, the effects of Mn and Ti co-doping on the physical and electrochemical properties of $LiNiO_2$ cathode material for lithium-ion batteries were investigated. It was found that Ti doping enhanced the structural stability, and cycling stability of Mn-doped $LiNiO_2$ while maintaining its high-capacity potential. The co-doped material, MnTi25, delivered a capacity of 190.8 mAh/g in full cells against a graphite anode, with a capacity retention of 93.7% after 50 cycles. The MnTi25 material also exhibited a remarkable rate capability, retaining over 85.5% of its capacity when the current density was increased by 40 times. These results indicate that MnTi25 can be a promising cathode material for high-performance lithium-ion batteries, by modifying the material's structure through co-doping. This study contributes to developing Ni-rich cathodes, advancing the potential of lithium-ion batteries for next-generation energy storage applications.

5. Future Works

The present study successfully demonstrates that co-doping the LNO material with Mn and Ti leads to significant improvements in its structural and electrochemical properties. These results pave the way for further exploration of the influence of varying Mn and Ti dopant ratios. Optimization of this dopant ratio represents a promising avenue for achieving superior performance characteristics. Future work will involve

the synthesis of LNO materials with a systematic variation in the Mn:Ti ratio. These materials will be carefully characterized to determine the optimal dopant ratio that maximizes the desired structural and electrochemical properties. In addition, the performance of these optimized LNO cathodes will be evaluated in various battery configurations, including different electrolytes and cell designs. This comprehensive approach will not only provide valuable insights into the structure-property relationships in Mn-Ti co-doped LNO, but will also guide the development of high-performance lithium-ion battery cathodes.

6. Acknowledgements

EO would like to thank TUBITAK for funding his research with the 2219 International Postdoctoral Research Fellowship Program for Turkish Citizens. The authors thank NSERC and Tesla Canada for the funding under the auspices of the Alliance Grants program.

7. Credit Authorship Contribution Statement

Erdinc Oz: Conceptualization, Data curation, Formal analysis, Investigation, Methodology, Validation, Visualization, writing – original draft, Writing - review & editing. Jeff Dahn: Investigation, Supervision, Review & editing.

8. Ethics Committee Approval and Conflict of Interest

The authors declare that they have no known competing financial interests or personal relationships that could have appeared to influence this work.

9. References

[1] J. R. Dahn, U. von Sacken, and C. A. Michal, “Structure and electrochemistry of Li1±yNiO2 and a new Li2NiO2 phase with the Ni (OH)2 structure,” Sol. State Ion, vol. 44, no. 1–2, pp. 87–97, Dec. 1990.
[2] C. S. Yoon, D. W. Jun, S. T. Myung, and Y. K. Sun, “Structural Stability of LiNiO2 Cycled above 4.2 v,” ACS Ener. Lett, vol. 2, no. 5, pp. 1150–1155, May 2017.
[3] J. Xu et al., “Elucidation of the surface characteristics and electrochemistry of high-performance LiNiO2,” Chem. Comm., vol. 52, no. 22, pp. 4239–4242, Mar. 2016.
[4] J. Xu et al., “Understanding the degradation mechanism of lithium nickel oxide cathodes for Li-ion batteries,” *ACS* Appl Mater Inter., vol. 8, no. 46, pp. 31677–31683, Nov. 2016.
[5] J. N. Reimers, E. Rossen, C. D. Jones, and J. R. Dahn, “Structure and electrochemistry of LixFeyNi1-yO2,” Sol. State Ion, vol. 61, no. 4, pp. 335–344, Jun. 1993.
[6] T. Ohzuku, A. Ueda, and M. Kouguchi, “Synthesis and Characterization of LiAl1 / 4Ni3 / 4 O 2 (R 3̄m) for Lithium-Ion (Shuttlecock) Batteries,” J. Electr. Soc, vol. 142, no. 12, pp. 4033–4039, Dec. 1995.
[7] A. Rougier, I. Saadoune, P. Gravereau, P. Willmann, and C. Delmas, “Effect of cobalt substitution on cationic distribution in LiNi1 − y CoyO2 electrode materials,” Sol. State Ion, vol. 90, no. 1–4, pp. 83–90, Sep. 1996.
[8] H. J. Kweon, S. J. Kim, and D. G. Park, “Modification of LixNi1−yCoyO2 by applying a surface coating of MgO,” *J* Pow. Sour., vol. 88, no. 2, pp. 255–261, Jun. 2000.
[9] H. Omanda, T. Brousse, C. Marhic, and D. M. Schleich, “Improvement of the Thermal Stability of LiNi0.8Co0.2 O 2 Cathode by a SiO x Protective Coating,” J. Electr. Soc, vol. 151, no. 6, p. A922, May 2004.
[10] J. Cho, T.-J. Kim, J. Kim, M. Noh, and B. Park, “Synthesis, Thermal, and Electrochemical Properties of AlPO4-Coated LiNi0.8Co0.2 O 2 Cathode Materials for a Li-Ion Cell,” J. Electr. Soc, vol. 151, no. 11, p. A1899, Oct. 2004.
[11] H. Qian et al., “Surface Doping vs. Bulk Doping of Cathode Materials for Lithium-Ion Batteries: A Review,” Elect. Ener. Rev., vol. 5, no. 4, pp. 1–32, Nov. 2022.

[12] T. F. Yi, X. Y. Li, H. Liu, J. Shu, Y. R. Zhu, and R. S. Zhu, "Recent developments in the doping and surface modification of LiFePO4 as cathode material for power lithium ion battery," Ion. (Kiel), vol. 18, no. 6, pp. 529–539, Jun. 2012.
[13] M. Y. Song, C. K. Park, S. Do Yoon, H. R. Park, and D. R. Mumm, "Electrochemical properties of LiNi1−yMyO2 (M = Ni, Ga, Al and/or Ti) cathodes," Ceram Int, vol. 35, no. 3, pp. 1145–1150, Apr. 2009.
[14] L. Shen et al., "Cobalt-free nickel-rich cathode materials based on Al/Mg co-doping of LiNiO2 for lithium ion battery," J. Coll. Inter. Sci, vol. 638, pp. 281–290, May 2023.
[15] H. Arai, S. Okada, Y. Sakurai, and J. Yamaki, "Electrochemical and Thermal Behavior of LiNi1 − z M z O 2 (M = Co , Mn , Ti) ," J. Electr. Soc, vol. 144, no. 9, pp. 3117–3125, Sep. 1997.
[16] L. Mu et al., "Structural and Electrochemical Impacts of Mg/Mn Dual Dopants on the LiNiO2 Cathode in Li-Metal Batteries," ACS Appl Mat. Inter., vol. 12, no. 11, pp. 12874–12882, Mar. 2020.
[17] H. Arai, S. Okada, Y. Sakurai, and J. Yamaki, "Electrochemical and Thermal Behavior of LiNi1 − z M z O 2 (M = Co , Mn , Ti) ," J. Electr. Soc, vol. 144, no. 9, pp. 3117–3125, Sep. 1997.
[18] H. Yang et al., "Simultaneously Dual Modification of Ni-Rich Layered Oxide Cathode for High-Energy Lithium-Ion Batteries," Adv Funct Mater, vol. 29, no. 13, p. 1808825, Mar. 2019.
[19] J. Kim and K. Amine, "The effect of tetravalent titanium substitution in LiNi1−xTixO2 (0.025⩽x⩽0.2) system," Electr. Comm., vol. 3, no. 2, pp. 52–55, Feb. 2001.
[20] Z. Xu et al., "Effects of precursor, synthesis time and synthesis temperature on the physical and electrochemical properties of Li(Ni1−x−yCoxMny)O2 cathode materials," J. Pow. Sour., vol. 248, pp. 180–189, Feb. 2014.
[21] T. Ohzuku, A. Ueda, and M. Nagayama, "Electrochemistry and Structural Chemistry of LiNiO2 (R3m) for 4 Volt Secondary Lithium Cells," J. Electr. Soc, vol. 140, no. 7, pp. 1862–1870, Jul. 1993.
[22] R. A. Yuwono et al., "Evaluation of LiNiO2 with minimal cation mixing as a cathode for Li-ion batteries," Chem.l Eng. Jour., vol. 456, p. 141065, Jan. 2023.
[23] R. D. Shannon and IUCr, "Revised effective ionic radii and systematic studies of interatomic distances in halides and chalcogenides," 0567-7394, vol. 32, no. 5, pp. 751–767, Sep. 1976.
[24] T. Xu, F. Du, L. Wu, Z. Fan, L. Shen, and J. Zheng, "Boosting the electrochemical performance of LiNiO2 by extra low content of Mn-doping and its mechanism," Electr. Acta, vol. 417, p. 140345, Jun. 2022.
[25] W. Li, J. N. Reimers, and J. R. Dahn, "In situ x-ray diffraction and electrochemical studies of Li1−xNiO2," Sol. State Ion, vol. 67, no. 1–2, pp. 123–130, Dec. 1993.
[26] H. Arai, S. Okada, Y. Sakurai, and J. I. Yamaki, "Reversibility of LiNiO2 cathode," Sol. State Ion, vol. 95, no. 3–4, pp. 275–282, Mar. 1997.
[27] C. S. Yoon et al., "Cation Ordering of Zr-Doped LiNiO2 Cathode for Lithium-Ion Batteries," Chem. of Mat., vol. 30, no. 5, pp. 1808–1814, Mar. 2018.
[28] U. H. Kim et al., "Microstructure-Controlled Ni-Rich Cathode Material by Microscale Compositional Partition for Next-Generation Electric Vehicles," Adv Ener. Mater, vol. 9, no. 15, p. 1803902, Apr. 2019.
[29] H. H. Ryu, K. J. Park, C. S. Yoon, and Y. K. Sun, "Capacity fading of ni-rich li[NixCoyMn1-x-y]O2 (0.6 ≤ x ≤ 0.95) Cathodes for High-Energy-Density Lithium-Ion Batteries: Bulk or Surface Degradation?," Chem. of Mat., vol. 30, no. 3, pp. 1155–1163, Feb. 2018.
[30] H. H. Ryu, G. T. Park, C. S. Yoon, and Y. K. Sun, "Suppressing detrimental phase transitions via tungsten doping of LiNiO2 cathode for next-generation lithium-ion batteries," J. Mat. Chem A Mater, vol. 7, no. 31, pp. 18580–18588, Aug. 2019.
[31] Y. Yao, "The effect of electrochemically inactive Ti substituted for Ru in Li2Ru1-xTixO3 on structure and electrochemical performance," Jour. of Ener. Chem. , vol. 60, pp. 222–228, Sep. 2021.
[32] B. Zong, "Influence of Ti doping on microstructure and electrochemical performance of LiNi0.5Mn1.5O4 cathode material for lithium-ion batteries," Mater Today Commun, vol. 24, p. 101003, Sep. 2020.